

Effect of Quarterly Element Addition of Cobalt on Phase Transformation Characteristics of Cu-Al-Ni Shape Memory Alloys



SAFAA NAJAH SAUD, TUTY ASMA ABU BAKAR, ESAH HAMZAH, MUSTAFA KHALEEL IBRAHIM, and ABOLLAH BAHADOR

In the current study, a new type of Cu-based shape memory alloys with the function of shape memory effect was successfully produced with the introduction of high-purity Co precipitates between the phases of Cu-Al-Ni shape memory alloy. The microstructure, transformation characteristics, and mechanical properties were systematically investigated by means of differential scanning calorimetry, field emission scanning electron microscopy, energy dispersive spectroscopy (EDS), transmission electron microscopy, X-ray diffraction (XRD), a tensile test, a hardness test, and a shape memory effect test. The typical microstructures show that a new phase was formed, known as the γ_2 phase, and the volume fraction and the size of this phase were gradually increased with the increasing Co content. According to the results of the XRD and EDS, it was confirmed that the γ_2 phase represents a compound of $\text{Al}_{75}\text{Co}_{22}\text{Ni}_3$. However, the presence of γ_2 phase in the modified alloys was found to result in an increase of the transformation temperatures in comparison with the unmodified alloy. Nevertheless, it was found that with 1 wt pct of Co addition, a maximum ductility of 7 pct was achieved, corresponding to an increase in the strain recovery by the shape memory effect to 95 pct with respect to the unmodified alloy of 50 pct.

DOI: 10.1007/s11661-015-2924-2

© The Minerals, Metals & Materials Society and ASM International 2015

I. INTRODUCTION

SHAPE memory alloys (SMAs) are intelligent materials that can undergo martensitic phase transformations when thermomechanical loads are applied and are able to recover their original shape when heated above a certain temperature.^[1,2] The martensitic transformation that occurs for the transformation of austenite (high-temperature phase) \rightleftharpoons martensite (low-temperature phase) is the main feature responsible for the characteristics of SMAs, *e.g.*, shape memory effect and pseudoelasticity. Many alloys are capable of exhibiting these properties, such as NiTi, and Cu-based and Fe-based alloys.^[3] As a result of their inexpensive, wide-ranging transformation temperatures, as well as their ease of production, high thermal stability, and small hysteresis with an affordable shape memory effect, Cu-based SMAs have attracted much attention from scientists and researchers. Among the Cu-based alloys, Cu-Al-Ni SMAs are the most used alloys, particularly whenever high temperatures are required. As such, they are assigned to high transformation temperatures that are able to work at or near 473 K (200 °C),^[4] which is

usually difficult for Cu-Zn-Al and NiTi alloys,^[5,6] maximum temperatures of which are around 373 K (100 °C).^[7] On the other hand, Cu-Al-Ni SMAs suffer from high brittleness,^[7] which is associated with large elastic anisotropy, intergranular cracking, and large grain size.^[8,9] To overcome these particular problems, two methods have been identified by the researcher thus far: the addition of the alloying elements or heat/aging treatment^[10–13] to control grain size; this has an effect on the mechanical properties.^[7,14] Therefore, to reduce brittleness, which is one of the most important defects of Cu-Al-Ni SMAs, Itsumi *et al.*^[15] replaced 2 pct of the aluminum content with Mn, which suppressed the eutectoid reaction $\beta_1 \rightarrow \alpha + \gamma_2$; Mn does not reduce the transformation temperature. At the same time, they used 1 pct of the Ti, which resulted in grain refinement; thus, intergranular cracking can be eliminated. Morris^[16] found that by adding the boron to the Cu-Al-Ni SMAs, the ductility increased. This can also be attributed to the presence of the boride particle. Another relevant point is that boron's addition can have an effect on the fracture mode, as it has been transferred from a brittle failure to an intergranular and transgranular failure. In another study, the same author^[10] found that the values of yield stress, microhardness, and tensile strength increase when the percentage of boron addition is increased. Adachi^[17] revealed that the Ti-doped Cu-Al-Ni SMA can reduce grain size and can enhance the mechanical properties. There are multiple studies on the effect of microalloying additions of Ti, Ni, Mn, B, Zr, Fe, CNTs, and Zn on the structure and mechanical

SAFAA NAJAH SAUD, Postdoctoral Research Fellow, TUTY ASMA ABU BAKAR, Senior Lecturer, ESAH HAMZAH, Professor, MUSTAFA KHALEEL IBRAHIM and ABOLLAH BAHADOR, Ph.D. Candidates, are with the Faculty of Mechanical Engineering, Universiti Teknologi Malaysia (UTM), 81310 Johor Baharu, Johor, Malaysia. Contact e-mail: tuty@mail.fkm.utm.my

Manuscript submitted October 28, 2014.

Article published online May 8, 2015

properties of Cu-Al.^[14,16,18–22] However, the effect of the addition of Co on microstructure, and on the mechanical properties of Cu-Al-Ni alloy, has not been reported elsewhere. However, the enhancement of mechanical properties such as ductility and shape memory are affected by controlling the grain size, degree of order, precipitate formations, structure, and morphology of the existing phases. Therefore, the current paper aims to investigate the effects of various additions of Cobalt on the microstructures, transformation characteristics, and mechanical properties of Cu-11.9 wt pct, Al-4 wt pct Ni SMA.

A. Experimental Procedures

1. Material preparation

The specified alloy was produced by melting the highest-purity metals of Cu (99.999 pct), Al (99.999 pct), Ni (99.95 pct), and Co (99.5 pct) using an induction furnace. These metals were melted in a silicon carbide crucible at a temperature of about 1573 K (1300 °C) under continuous stirring, and were then poured into a cast iron mold with dimensions of 270 mm × 50 mm × 20 mm. The ingot was cut into the required sample dimensions using EDM wire, homogenized at 1173 K (900 °C) for 30 minutes, and then quenched in water, which led to the formation of martensite. The chemical composition for the Cu-Al-Ni-Co SMAs was investigated using inductively coupled plasma mass spectrometry (ICP-MS). These results are shown in Table I.

B. Material Characterization

Flat specimens were cut from the aged samples with dimensions of 10 mm × 10 mm × 2 mm for the microstructural and XRD characteristics. Transmission electron microscopy (TEM) characterization in a JEM2010 operated at 200 kV was also used to investigate the microstructural changes. Filings of the alloys removed were from 2 to 6 mg, and were taken for differential scanning calorimeter measurements using a Mettler Toledo DSC 822e; the scanning rate was 10 K/min within the 450 K through 573 K (177 °C to 300 °C) range. The phase identifications and crystal structure determinations were carried out using a D5000 Siemens X-Ray diffractometer fitted with a CuK_α X-ray source in a locked couple mode, a 2θ range of between 30 and 80 deg, and a 0.05 deg/s scanning step. The quenched samples were ground and polished and then etched in a solution containing 2.5 g ferric chloride acid (FeCl₃·6-

H₂O) and 48 mL methanol (CH₃OH) in 10 mL HCl for 4 minutes.^[23–25]

C. Mechanical Tests

1. Tensile and hardness tests

The tensile test was performed using an Instron 5982-type universal testing machine operated at a constant strain rate of 0.1 mm/min. The tests were carried out at room temperature until a failure occurred, and then the fracture stress–strain was determined under the tensile load. The purpose of this test was to optimize the elastic and plastic area ranges before performing the shape memory effect test. Vicker’s microhardness test was performed with 10 kg for 25 seconds to measure the hardness of these alloys.

2. Shape memory effect test

The shape memory effect test was carried out using a specially designed machine as shown in Figure 1. The specially designed contents were analyzed using an Instron 5982-type universal testing machine, operated with special program parameters according to the shape memory test, which was connected with heater tape and digital thermocouple to control the applied temperature, as well as an external extensometer to measure the shape extension and recovery. The tests were carried out at a temperature below M_f, which was about 373 K (100 °C), where the alloys would be able to obtain shape recovery. Then, the deformed sample that still had an unrecoverable shape was subsequently heated above the austenite finish temperature (A_f+ 333 K (60 °C)) for 10 minutes, followed by water quenching to recover the residual strain (ε_r). The recovered shape was attributed to the transformation of the detwinned martensite to the austenite phase, which had been termed as transformation strain (ε^t). After the cooling process, the martensite again formed into a self-accommodated structure.

II. RESULTS AND DISCUSSION

A. Microstructural Observations

Optical microscopy (left-hand side) and field emission scanning electron microscopy (FE-SEM) (right-hand side) in Figure 2 show the microstructures of Cu-Al-Ni SMAs before and after the Co additions. The martensite formed completely in the structure of each sample after homogenization treatment. The martensite formed in two morphologies: needle-like and plate-like. A number of studies clearly show that the martensite is generally formed in two different types of structures: (i) self-accommodating martensite stacking structure and (ii) stress-induced martensite with a monopartial stacking structure.^[26] The morphology of the self-accommodating martensite exhibits a plate-like structure, which is also called the lath structure, and has a diamond-shaped morphology that can produce a long, layered structure.^[27] There are six types of groups that can be generated in the self-accommodating martensite, and

Table I. Chemical Compositions of the Alloys (Mass Fraction, Weight Percent)

Alloy	Cu	Al	Ni	Co
1	84.1	11.9	4	—
2	83.7	11.9	4	0.4
3	83.4	11.9	4	0.7
4	83.1	11.9	4	1

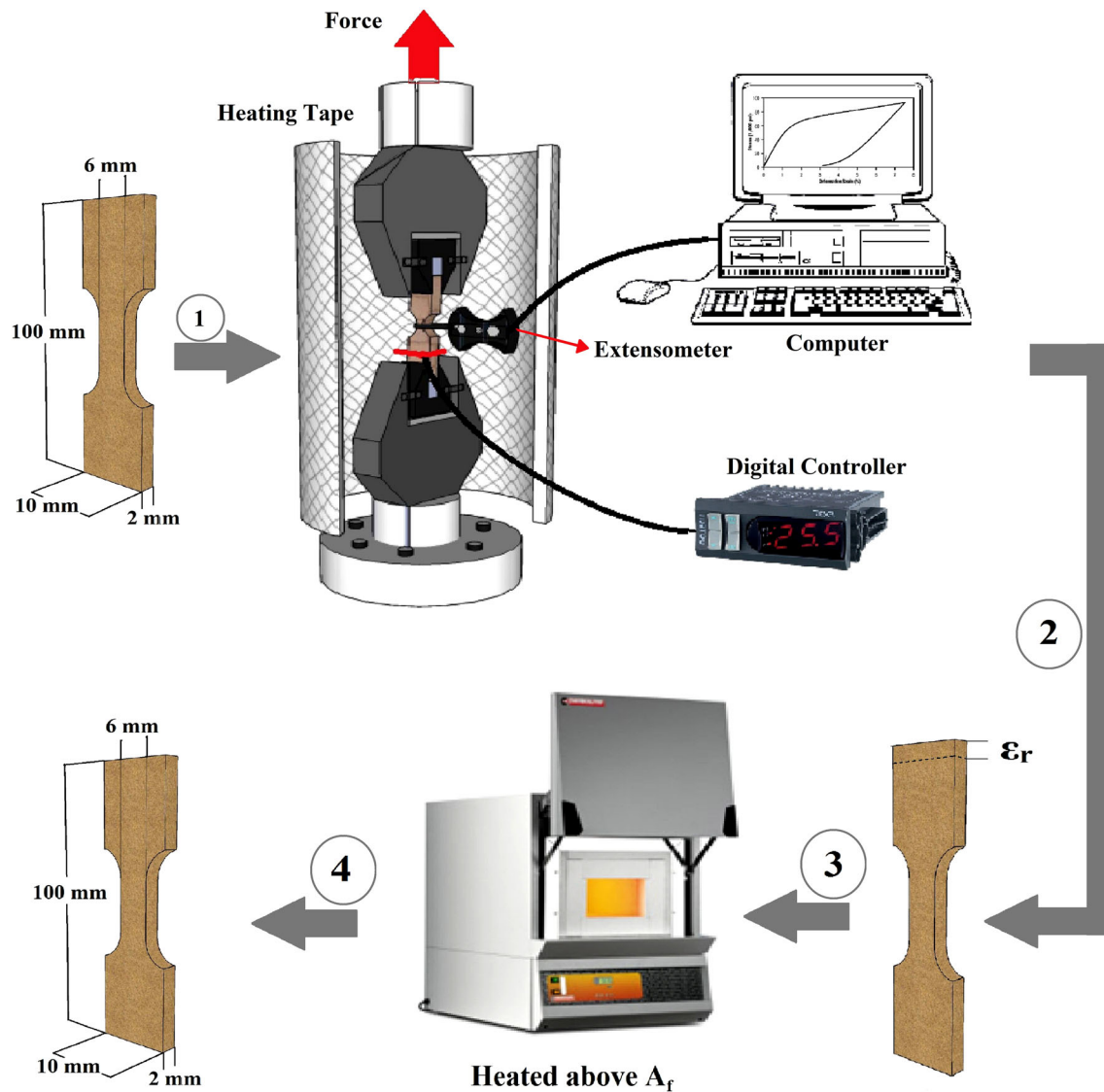


Fig. 1—Schematic illustration of the shape memory effect test.

each group contains four variants. When these variant groups are combined, a nearly zero macroscopic morphology change can be generated.^[27,28] The most characteristic feature of the martensitic microstructures in noble metal copper-based ternary alloys such as Cu-Zn-Al, Cu-Al-Mn, or Cu-Al-Ni is the prevalence of groups of essentially parallel-sided plates and the occurrence of comparatively a few large groups of unique orientation within the grains of the parent phase.^[28] Based on the mechanisms of martensite variants, the alloys have the ability to deform at low stress levels and, moreover, can perform the shape memory effect. The formation of the martensite plate-like structure can demand either thin layer and parallel-sided plates or grow in two or four plate-like structures that contact as a group to produce a self-accommodating system crisscross plate-like structure of which is formed with the matrix, which is termed as conventional habit planes, while the internal junction planes are referred to as a twin martensite plane.^[28,29]

From Figures 2(a) and (b), it is clear that the microstructure consists of two types of martensite that are formed: β_1' with an 18R structure and γ_1' with a 2H structure. The γ_1' , exhibiting a parallel martensite morphology, probably has a lath-like structure^[2]; these particular kinds of lath morphologies have also grown into grain, even while the β_1' phase is typically formed with self-accommodating groups in two distinct morphologies: plate-like and needle-like in martensitic conditions.^[8] The self-accommodated martensite plate-like groups are formed in the as-quenched condition. It has been reported that grains grow with further annealing.^[28] Perhaps it seems that with the Co addition, an innovative new phase is formed and begins to grow up into the matrix and consequently above the needle-like and plate-like structures of β_1' phases, which are typically known as the γ_2 phase. Figures 2(c) and (d) show that the microstructure of the Cu-Al-Ni-0.4 wt pct Co alloy consists of mainly the β_1' phase, where the

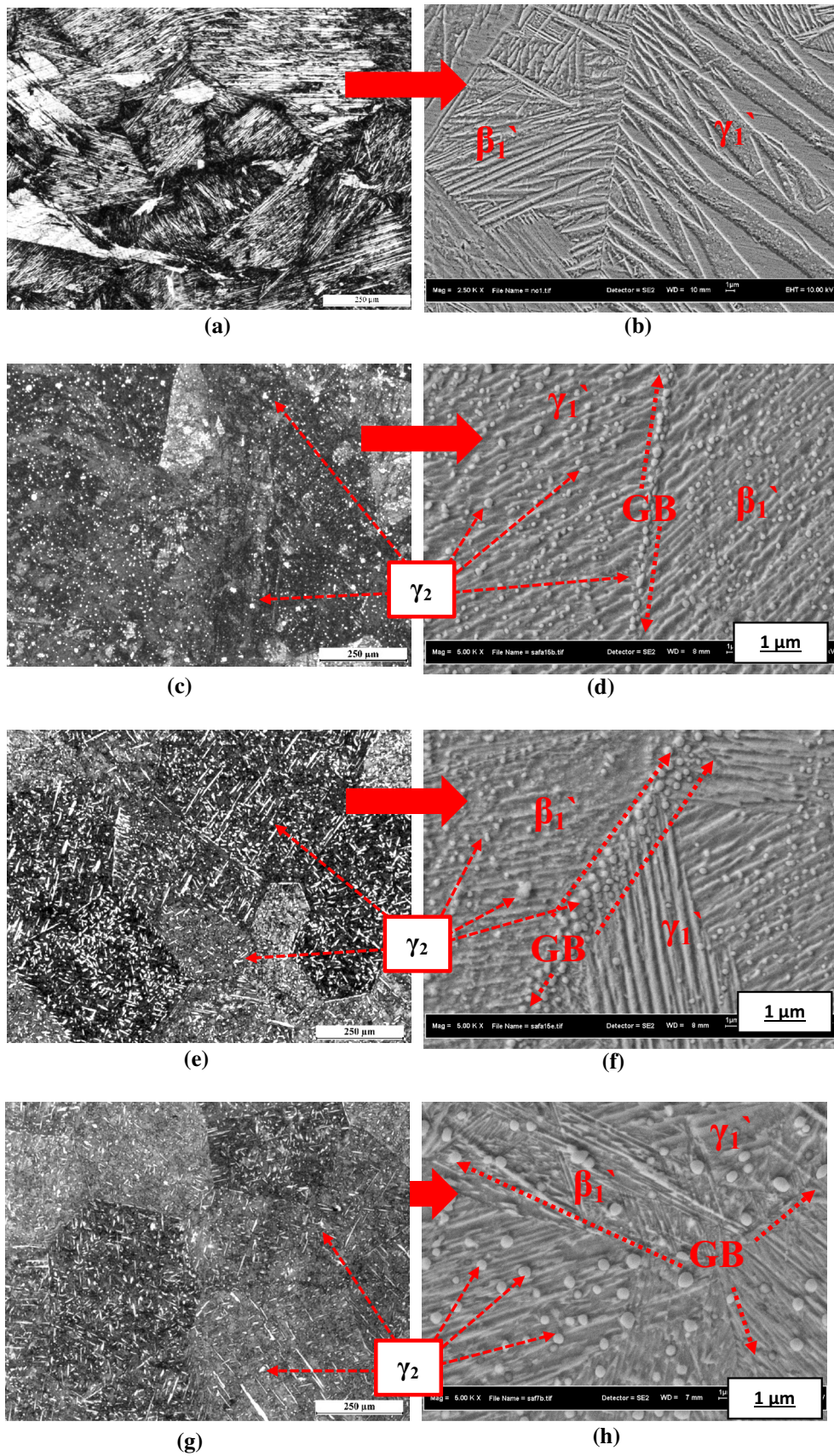


Fig. 2—Optical (left-hand side) and FESEM (right-hand side) micrographs showing the microstructures of the Cu-Al-Ni SMA with different concentrations of Co addition: (a, b) Cu-Al-Ni, (c, d) Cu-Al-Ni-0.4 wt pct Co, (e, f) Cu-Al-Ni-0.7 wt pct Co, (g, h) Cu-Al-Ni-1 wt pct Co.

thicknesses of needle-like and plate-like structures become thinner than the base alloy, and the γ_2 phase starts to agglomerate at the grain boundaries with a longitu-

dinal axis in the casting direction, leading to the development of important anisotropic properties. Once a significant amount of Co increases from 0.4 to

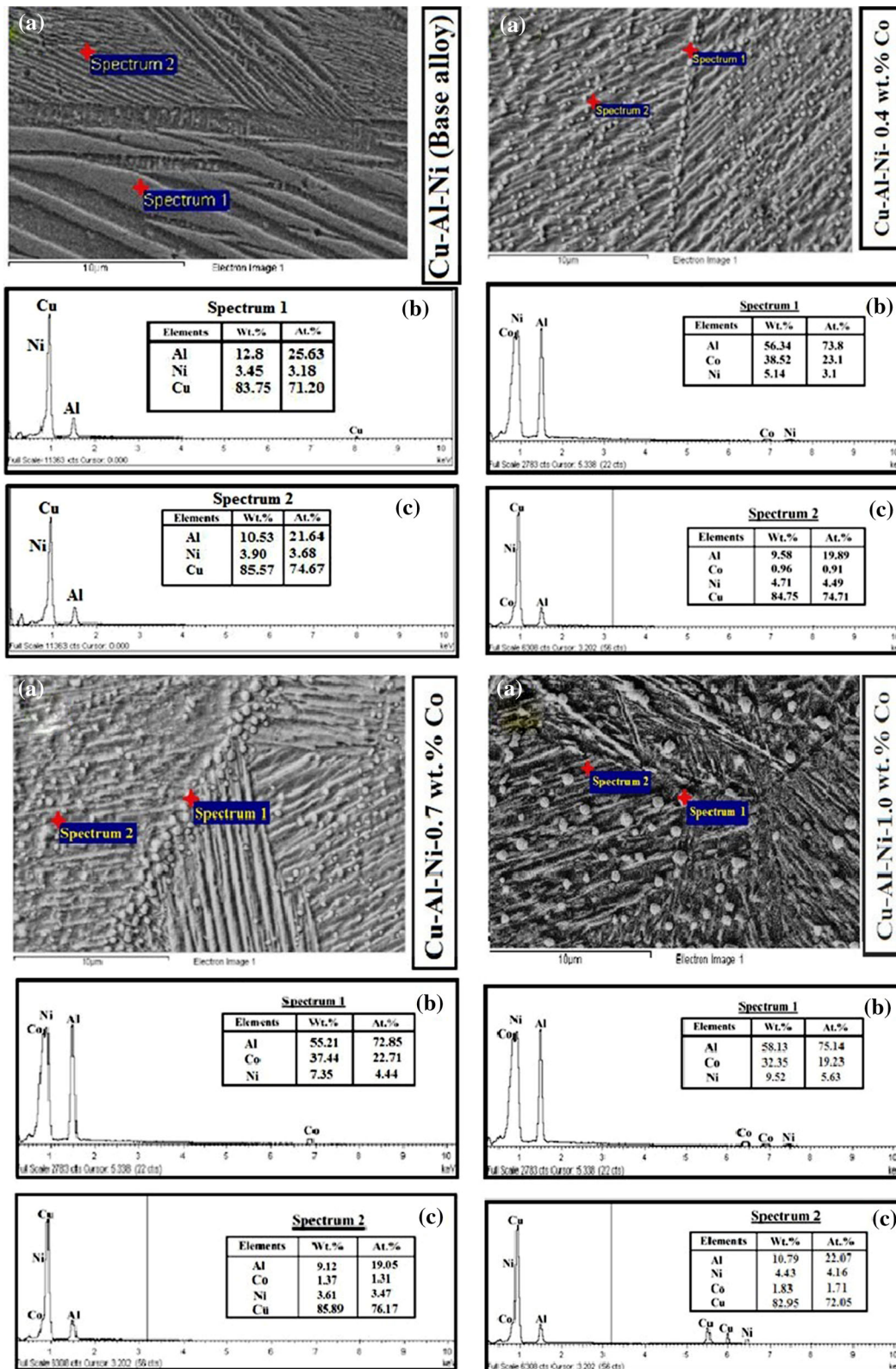


Fig. 3—A spot scanned during the EDS analysis of the Cu-Al-Ni-0.4 wt pct Co: (a) Micrograph of scanned area; (b) Spectrum 1; (c) Spectrum 2.

0.7 wt pct, the γ_2 phase evolves into consistent spherical-shaped particles, and their area fraction increases to be 11.6 pct together with an ordinary particle size of 0.4 through 0.5 μm . Furthermore, the γ_2 phase begins to diffuse from the matrix in the direction of the grain boundaries that make them come across as thicker than Cu-Al-Ni-0.4 wt pct Co SMA as shown in Figures 2(e) and (f). Moreover, as a result of increases in the addition of Co amount, the thickness of the β_1' phase increased and orientated in different directions as indicated by small arrows (1, 2, and 3) in Figure 2(f). The grain boundaries became much clearer, and the thickness of the β_1' phase increased more than those of Cu-Al-Ni-0.4 wt pct Co and Cu-Al-Ni-0.7 wt pct Co alloys, and consequently, the orientations of the β_1' phase changed from grain to grain as shown in Figure 2(h). Due to this fact, the γ_2 phase evolves more consistently in shape and more prominently in size with Co additions. The effects of Co additions on the morphologies and orientations of the γ_2 phase are vital to the response to the transition of the morphology γ_2 phase from nonuniform particles to the spherical-shaped particles. In accordance with an EDS analysis of a spot scanned for the γ_2 -phase area, it was found that these precipitates are Co-rich; they are an amalgamation of Co, Ni, and Al in a compound of $\text{Al}_{75}\text{Co}_{22}\text{Ni}_3$, as pointed out in Figure 3. However, the area fraction and precipitate size of γ_2 phase were estimated according to the phase color contrast performed using specific software, known as ImageJ. It was found that the increase in the amount of Co addition leads to increases in the area fraction and the size of the γ_2 phase. For instance, when Co addition was increased to 1 wt pct, the area fraction and the particle size of γ_2 phase increase to 15.63 pct and 0.68 μm , respectively, as shown in Figure 4.

With the purpose of showing the distribution of the alloying element, the FESEM along with elemental mapping was taken for Cu-Al-Ni-1 wt pct Co SMA, as shown in Figures 5(a) through (e). The elemental distribution of the Cu-Al-Ni-1 wt pct Co SMA (Cu, Al, and Ni) was homogenized, and the Co was distributed randomly in the matrix, as shown in Fig-

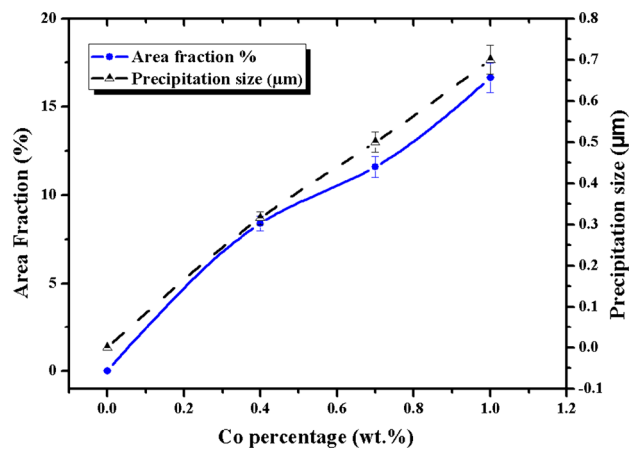


Fig. 4—Volume fraction and size of γ_2 precipitation of the Cu-Al-Ni- x Co (x is 0, 0.4, 0.7, and 1 wt pct).

ure 5(c). The phenomena attained after the Co amount increased to 1 wt pct started to diffuse into the matrix with the increase in the percentage of γ_2 -phase area fraction.

To verify the existence of γ_2 phase in the microstructure and their influence on the crystallite size of Cu-Al-Ni SMAs, the XRD diffraction patterns were utilized at room temperature; the scanned curves are shown in Figure 6. It was observed that a significant change happened in the current patterns after the Co was added compared with the base alloy; these changes are represented by shifting the peaks and by eliminating and increasing/decreasing the value of intensity, depending on the percentage of the Co additions. It has been noticed that the pattern peaks vary in terms of intensity, shape, and height. In addition, it was observed that three peaks were obtained (621), (712), and (314) after the addition, which confirmed the existence of the intermetallic compound of $\text{Al}_{75}\text{Co}_{22}\text{Ni}_3$ (γ_2 phase).

The lattice parameters and crystallite size of the Cu-Al-Ni SMA with and without addition were determined from the XRD patterns and recorded in Table II. The lattice parameters were evaluated in accordance with an orthorhombic 18R structure, which was proven by the XRD indexing patterns. Thus, the lattice parameters were determined using the following equation^[30]:

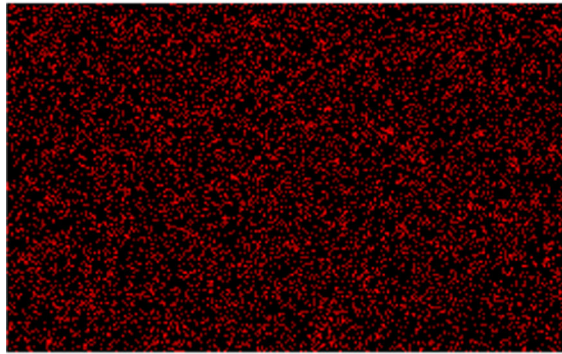
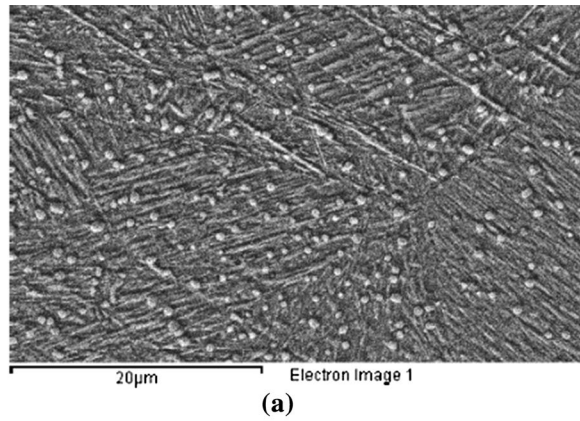
$$\frac{1}{d^2} = \frac{1}{a^2} \left[\frac{h^2}{\sin^2 \beta} \right] + \frac{k^2}{b^2} + \frac{1}{c^2} + \left[\frac{l^2}{\sin^2 \beta} \right] - \frac{2hl \cos \beta}{ac \sin^2 \beta}. \quad [1]$$

The ratio a/b is also calculated and presented in Table II, whereas this ratio for the base alloy and modified alloys was less than $\sqrt{3}/2$ in an ordered case due to the atomic sizes of the constituent atoms of the 18R martensite,^[31,32] which depended on the obtained results. The XRD of the alloys with a monoclinic structure was similar to earlier works.^[8,33] Although the XRD results showed similar characteristics, some of the diffraction pattern planes shifted in the location during the addition process. One of the most important factors that has a significant effect on martensitic transformation is the structure ordering.^[33,34] The crystallite size was determined by a Scherrer method,^[35,36] with the mean value of the main five peaks of (122), (0018), (128), (1210), and (208) being calculated as per the following equation:

$$\text{Crystallite size}(d) = \frac{0.9 * (\lambda)}{B * \cos \theta}. \quad [2]$$

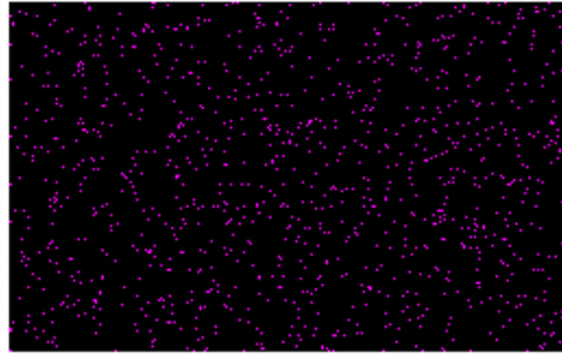
The broadening and shifting of the Bragg peaks indicate a reduction in the crystallite sizes during the Co additions as shown in Table II. This reduction may be attributed to the strain hardening and subsequent strain relaxation due to dynamic recovery caused by the agglomeration of precipitates at the grain boundaries, which led to restricted grain growth and, thus, to a reduction in crystallite size.

Figures 7(a) through (i) display the TEM images, HRTEM, and selected area diffraction of the Cu-Al-Ni, Cu-Al-Ni-0.7 wt pct Co and Cu-Al-Ni-1 wt pct Co



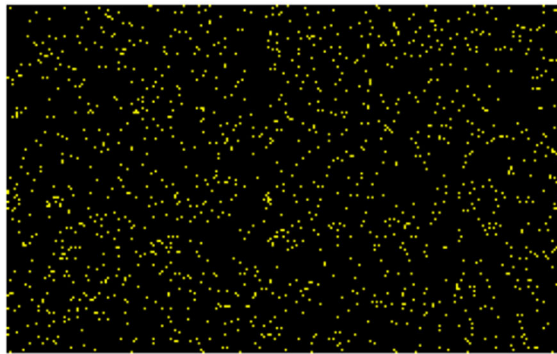
Al Ka1

(b)



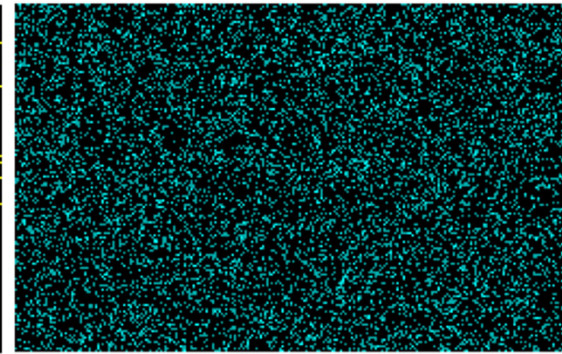
Co Ka1

(c)



Ni Ka1

(d)



Cu Ka1

(e)

Fig. 5—Elemental distribution map showing the distribution of Cu, Al, Ni, and Co in the Cu-Al-Ni-1 wt pct Co SMA.

SMA. The TEM image (Figure 7(a)) clearly reveals the existence of γ_1' and β_1' martensite in the microstructure. The HRTEM images in Figure 7(b) show the lattice fringes of the martensite phase. The SADP images show the diffraction patterns of the base alloy that presented a monoclinic structure, as shown in Figure 7(c), which is identical to the XRD results. The β_1 parent phase is first transformed into γ_1' twinned martensite; this transient or intermediate state of twinned martensite is further detwinned into a single corresponding variant by lattice invariant shear. Then, the γ_1' phase is transformed into the β_1' phase by a lattice distortion, and finally the slip shear (also lattice invariant shear) occurs inside the β_1' lattice.^[37,38] Although the steps above might not exactly correspond to the real transformation processes, they do describe the final deformation state of the β_1' martensite.

The examination of the area diffraction patterns reveals that the stacking sequence of the formed martensite is a monoclinic structure. Once Co is added, the morphology of the martensite phase change, in addition to the lattice fringes, varied in terms of d spacing and orientation, and these variations can easily and precisely clarify the shifting in the XRD peaks (Figure 6). The stacking sequence of martensite also confirmed a monoclinic structure along with different positions of the peaks as indicated in Figures 7(d) through (i).

B. Transformation Temperatures

Transformation temperatures of alloys were calculated using the software accompanying the DSC instrument. A_s , M_s , A_f , and M_f temperatures were determined

from the conventionally used extrapolated onset and offset temperatures. Although the use of extrapolating onset and offset temperatures was universal in the thermal analysis, where mostly chemical reactions rather than phase transformations have been studied, it might have been better to use onset and offset temperatures (point of deviation from baseline) rather than extrapolated temperatures for the interpretation of anomalous effects in DSC curves of diffusionless martensitic transformations. However, to prevent the subjectiveness of the choice of deviation point and obey the general trend in the DSC, extrapolated values were used.

Figures 8(a) through (d) show the DSC curves of the forward and reverse transformations of the Cu-Al-Ni SMAs with and without Co additions. The transformation temperatures A_s , A_f , M_s , and M_f are measured, and the data are tabulated in Table III. It was found that during the heating and cooling processes, the observed peaks shifted toward high transformation temperatures in addition to obtaining wide and low-intensity peaks compared with the base alloy. These shifting and shape variations are mainly dependent on the amount of Co additions. Furthermore, it was observed that as the amount of Co increased, the area fraction of the γ_2 phase increased, which can lead to a decrease in the intensity of the obtained peaks and make them wider than the base alloy. Furthermore, several small peaks occurred before and after the main peak on the cooling curve; however, these peaks were absent from the heating curve. These peaks are mainly attributed to

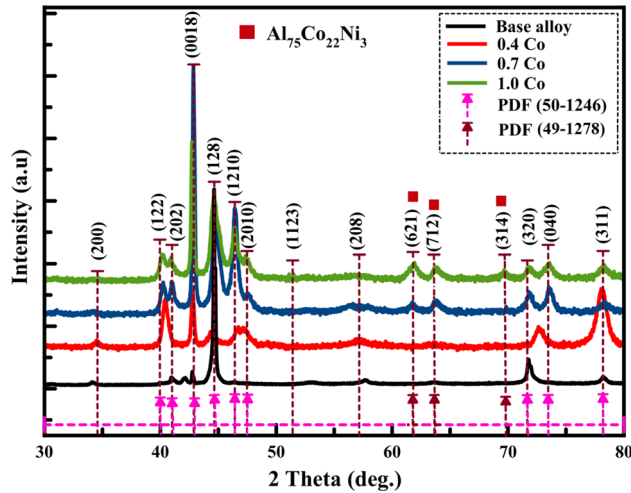


Fig. 6—X-ray diffraction patterns of (a) Cu-Al-Ni, (b) Cu-Al-Ni-0.4 wt pct Co, (c) Cu-Al-Ni-0.7 wt pct Co, (d) Cu-Al-Ni-1 wt pct Co.

Table II. Lattice Parameters and Crystallite Sizes of Cu-Al-Ni SMA With and Without Co Additions

Alloy	a (Å)	b (Å)	c (Å)	a/b	Crystallite Size (nm)
Cu-Al-Ni	4.425	5.250	38.055	0.84286	25.5
Cu-Al-Ni-0.4 wt pct Co	4.355	5.207	38.073	0.83637	16.3
Cu-Al-Ni-0.7 wt pct Co	4.428	5.249	37.985	0.84359	16.7
Cu-Al-Ni-1 wt pct Co	4.427	5.252	38.080	0.84292	17.4

Fig. 7—TEM images corresponding to selected area diffraction patterns of Cu-Al-Ni, Cu-Al-Ni-0.7 wt pct Co and Cu-Al-Ni-1 wt pct Co: (a) Bright field of TEM image of Cu-Al-Ni wt pct alloy, (b) HRTEM image of the Cu-Al-Ni wt pct Co alloy, (c) SADP of the Cu-Al-Ni wt pct Co alloy, (d) Bright field of TEM image of Cu-Al-Ni-0.7 wt pct alloy, (e) HRTEM image of the Cu-Al-Ni-0.7 wt pct Co alloy, (f) SADP of the Cu-Al-Ni-0.7 wt pct Co alloy, (g) Bright field of TEM image of Cu-Al-Ni-1 wt pct Co alloy, (h) HRTEM image of the Cu-Al-Ni-1 wt pct Co alloy, (i) SADP of the Cu-Al-Ni-1 wt pct Co alloy.

the occurrence of the intermartensitic transformations. Due to the residual stress, the intermartensitic transformations have been suppressed, which led to their elimination during the heating process.^{39,40} The austenite \rightleftharpoons martensite transformation temperatures vs the Co weight percentages are shown in Figure 9. The transformation temperatures (A_s , A_f , M_s , and M_f) gradually increased in tandem with the increase in Co amount.

The equilibrium temperature T_o between the parent phase and martensite phase when the Gibbs Free Energy (G) of both phases is equalized. Based on the following relations, the T_o was calculated as follows:

$$\begin{aligned} \Delta G^{M \rightarrow A}(T_o) &= G^A(T_o) - G^M(T_o) \\ &= (H^A - T_o S^A) - (H^M - T_o S^M) \\ &= \Delta H^{M \rightarrow A} - T_o \Delta S^{M \rightarrow A} \end{aligned} \quad [3]$$

Or

$$\begin{aligned} \Delta G^{A \rightarrow M}(T_o) &= G^M(T_o) - G^A(T_o) \\ &= (H^M - T_o S^M) - (H^A - T_o S^A) \\ &= \Delta H^{A \rightarrow M} - T_o \Delta S^{A \rightarrow M} \end{aligned} \quad [4]$$

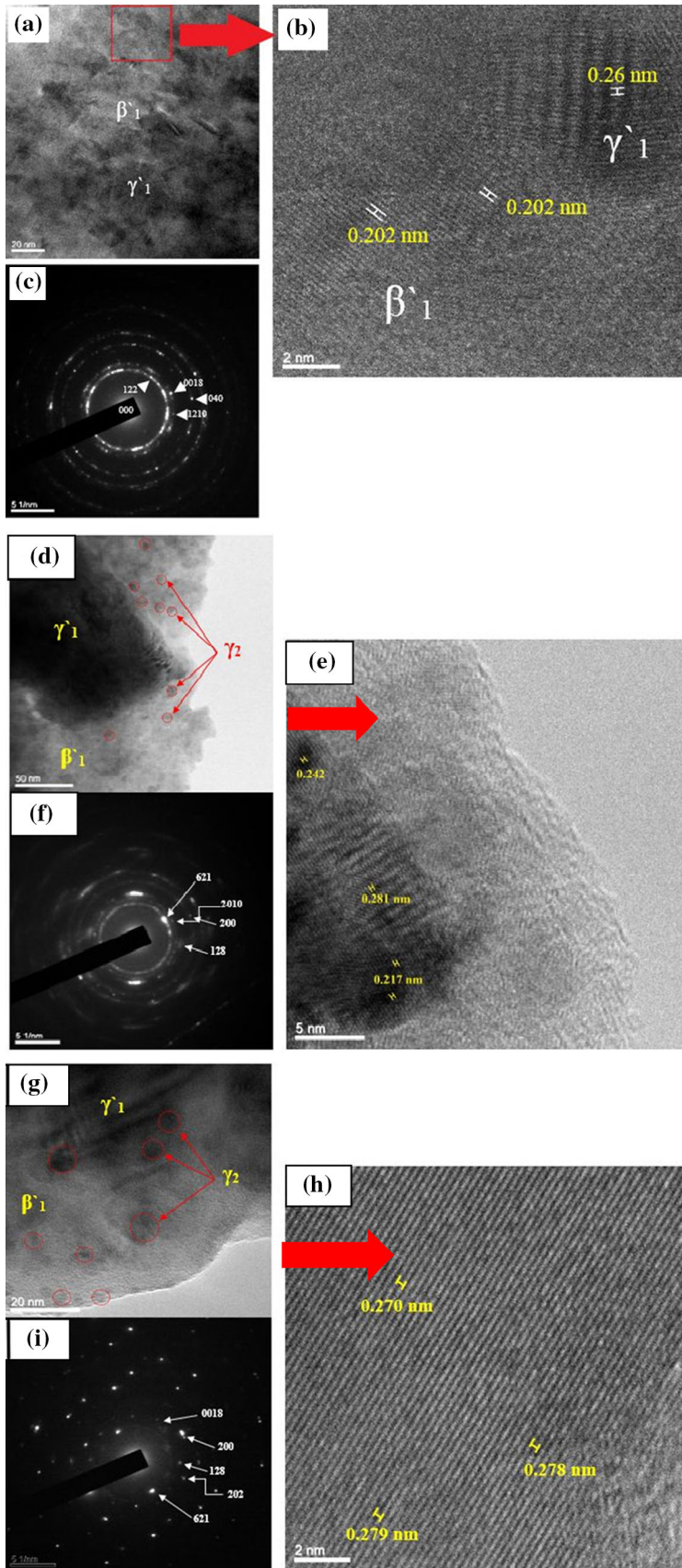
In addition, T_o , for the alloy, when the $\Delta G^{M \rightarrow A}(T_o)$ and $\Delta G^{A \rightarrow M}(T_o) = 0$ at $T = T_o$ is expressed as^[41,42]

$$T_o = \frac{\Delta H^{M \rightarrow A}}{\Delta S^{M \rightarrow A}} \text{ or } T_o = \frac{\Delta H^{A \rightarrow M}}{\Delta S^{A \rightarrow M}} \quad [5]$$

The equilibrium temperature between the austenite and martensite phase transformations can be expressed as follows:

$$T_o = \frac{1}{2}(M_s + A_f) \quad [6]$$

The T_o values were calculated before and after the additions, and the recorded data are listed in Table III, and it was found that the maximum value of T_o was observed with Cu-Al-Ni-1 wt pct Co. Moreover, the thermodynamic parameters of forward and reverse transformations were calculated and are presented in Table IV. The enthalpy and entropy of both transfor-



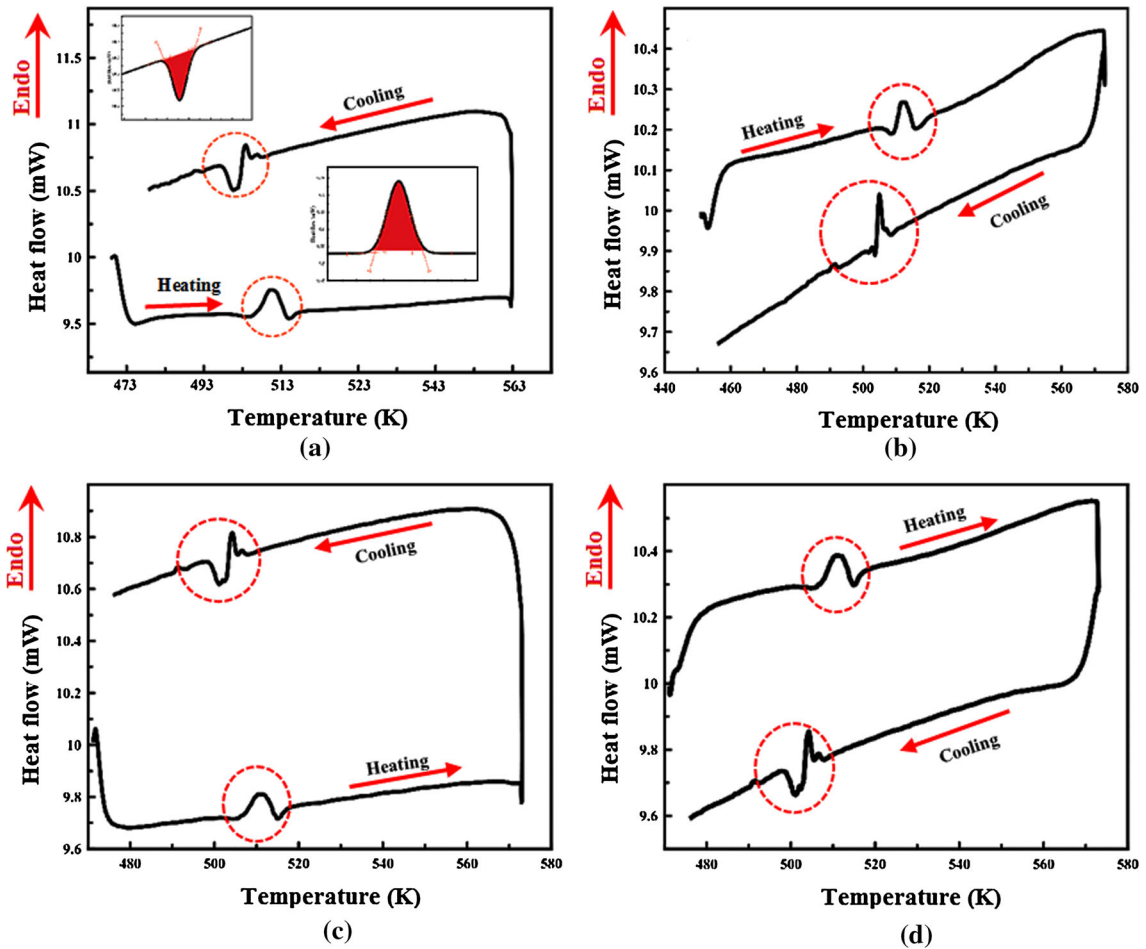


Fig. 8—DSC curves of the Cu-Al-Ni SMA with different percentages of Co addition: (a) Cu-Al-Ni; (b) Cu-Al-Ni-0.4 wt pct Co; (c) Cu-Al-Ni-0.7 wt pct Co; (d) Cu-Al-Ni-1 wt pct Co.

Table III. Transformation Temperatures of Cu-Al-Ni SMA With and Without Co Additions

Alloy	Transformation Temperatures				
	A_s (K)	A_f (K)	M_s (K)	M_f (K)	T_o (K)
Cu-Al-Ni SMA	506.9	515.1	503.3	496.5	509.2
Cu-Al-Ni-0.4 wt pct Co	513.4	521.5	510	505.3	515.75
Cu-Al-Ni-0.7 wt pct Co	515.68	525.2	514.2	507.7	519.7
Cu-Al-Ni-1 wt pct Co	522.88	532	521.2	514.4	526.6

mations obtained a minimum value with Cu-Al-Ni-0.4 wt pct Co, and then increased slightly due to the increasing Co addition.

C. Mechanical Test

1. Stress-strain behavior and hardness analysis

The typical stress-strain curves obtained from the tensile test are illustrated in Figure 10, and the calculated fracture stress and fracture strain are shown in Table V. The elongation of the Cu-Al-Ni SMA has been enhanced from 1.65 to 7 pct, and the tensile stress increased from 270 to 650 MPa after the Co addition.

These improvements are mainly attributed to the morphology of the martensite phase as well as to the area fraction of the γ_2 phase. As long as the volume fractions of β_1' and γ_2 phases increased, the mobility of dislocations decreased. Therefore, the dislocations are required to manage high stress for the purpose of shearing and/or bowing around these phases, and thus, to increase the strength of the alloys.

The tensile curves of the Cu-Al-Ni SMAs with and without Co additions are divided into two regions in accordance with the differences in the slope of each obtained curve. With the initial load, the alloys exhibited a classical feature of the SMAs along with a distinct

region, followed by a near plateau. The first stage (region I) represents the elastic deformation stage with a linear elastic behavior. Region II represents a near

plateau. This stage occurs due to the reorientation of the multivariant martensite, which results in the transformation of the deformation-induced martensite to martensite transformation. However, the alloys Cu-Al-Ni-0.4 wt pct Co, Cu-Al-Ni-0.7 wt pct Co, and Cu-Al-Ni-1 wt pct Co SMAs exhibit higher elongation and strength compared with the base alloy. This is attributed to the low volume fraction of γ_1' phase into the microstructure, thus making the reorientation of β_1' phase easier.

The fracture behaviors of the Cu-Al-Ni SMA with and without Co additions have been examined during the tensile test until fracture and is shown in Figures 11(a) through (d). The Cu-Al-Ni SMA has exhibited a brittle fracture mode with a maximum strain of 1.6 pct as shown in Figure 11(a). A common observation during the traditional casting process of Cu-Al-Ni SMA is the brittleness, which was confirmed by other researchers.^[43–45] Generally speaking, it is important to bear in mind that a crack is always initiated at the grain boundaries and propagated into the specimen at different angles according to the direction of the uniaxial tensile force, due to the high internal stresses in these regions. However, the principles behind the crack

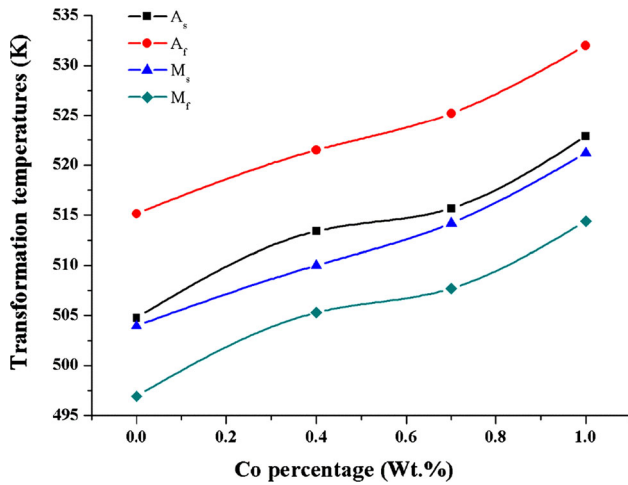


Fig. 9—Evaluation of the martensite–austenite transformation temperatures as a function of Co addition.

Table IV. Thermodynamic Parameters of Cu-Al-Ni SMA With and Without Co Additions

Alloy	$\Delta H_{\text{forward}}$ (J/g)	$\Delta H_{\text{reverse}}$ (J/g)	$\Delta S_{\text{forward}}$ (J/kg K)	$\Delta S_{\text{reverse}}$ (J/kg K)
Cu-A-Ni	1.528	6.473	1.371	5.808
Cu-Al-Ni-0.4 wt pct Co	1.29	0.69	2.51	1.34
Cu-Al-Ni-0.7 wt pct Co	1.60	1.11	3.04	2.11
Cu-Al-Ni-1 wt pct Co	2.07	1.53	3.99	2.95

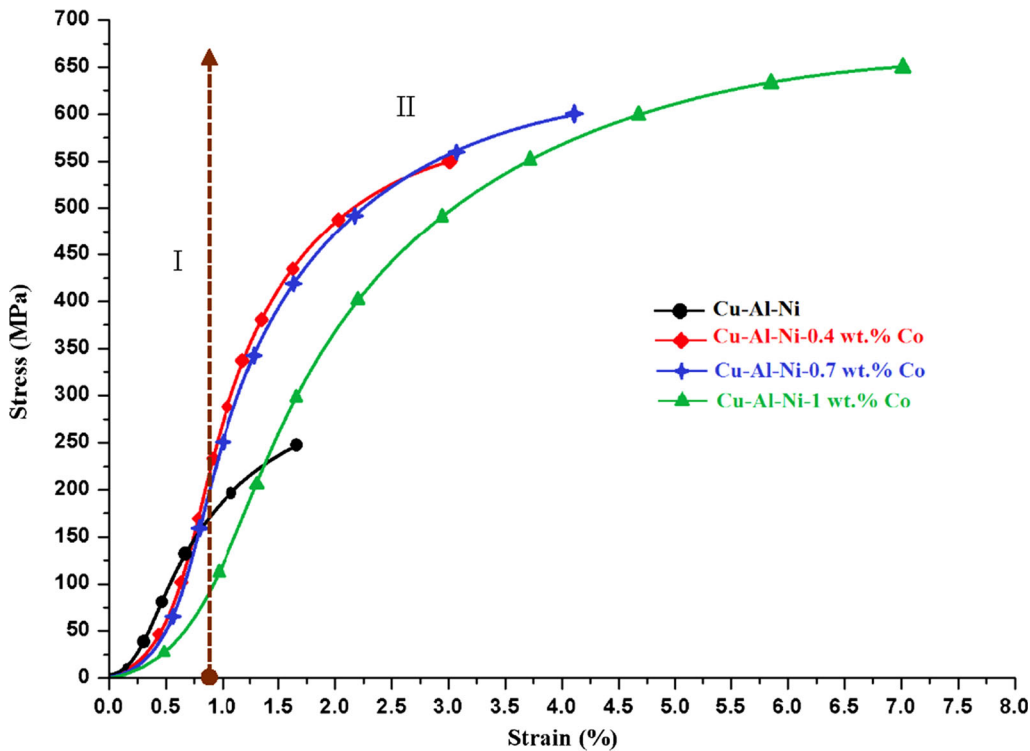


Fig. 10—Stress–strain curves obtained from the tensile test performed at room temperature.

propagation are that when the distribution of the stress is so complicated at these fold notes of the grain boundaries, the stress is not easily released during the deformation process. Thus, the cracks are initiated at these fold notes and start to propagate into the materials, some of the martensite is induced due to the crystal orientations related to the tensile axis. On the other part of the grains, the martensite is formed at the same stage of deformation.

Furthermore, there are many factors that can influence the propagation of cracks, and therefore, increase the strength of materials, such as the stress-induced martensite plate-like structures, the segregation of impurities at the grain boundaries, and high elastic anisotropy caused by the elastic and plastic strain incompatibilities at the grains. These attributes can

collectively preclude the propagation of cracks by changing the propagation path and/or by making the crack grow sufficiently large.^[43,46-48] For example, when the crack is large enough and an elastic anisotropy occurs, the stress concentrations at the crack tips are large enough to overcome the stress concentrations at the grain boundaries, and thus, crack propagation will be controlled. Accommodating and/or displacing the stress produced during the formation of the martensite-induced lead to a reduction in the size of the crack with a small orientation, and thereby, the prevention of intergranular cracks. When the Co was added, the fracture surfaces exhibited a transgranular feature along with rupture dimples distributed in the fractured area. This feature represents the enhancement of the ductility by converting the fracture feature from brittle to ductile

Table V. The Tensile, Hardness, and Shape Memory Tests on the Cu-Al-Ni SMA With and Without Co Additions

Alloy	Fracture Stress (σ^F) (MPa)	Fracture Strain (ϵ^F) (pct)	Hardness (MPa)	Strain Recovery by SME (ϵ_{SME}) (pct)
Cu-Al-Ni	270	1.65	253.6	50
Cu-Al-Ni-0.4 wt pct Co	550	3	273	70
Cu-Al-Ni-0.7 wt pct Co	600	4.1	329	83.3
Cu-Al-Ni-1 wt pct Co	650	7	345	95

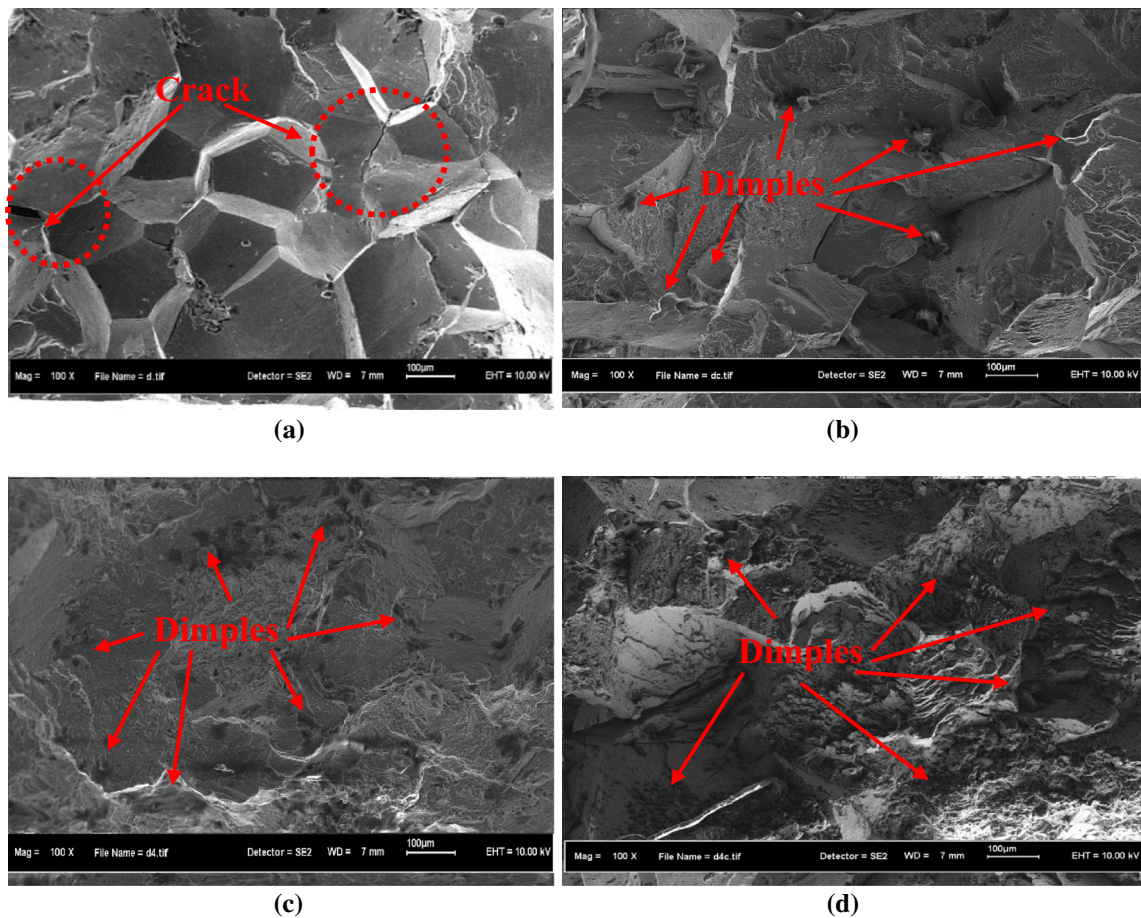


Fig. 11—Fracture surfaces: (a) Cu-Al-Ni SMA, (b) Cu-Al-Ni-0.4 wt pct Co SMA, (c) Cu-Al-Ni-0.7 wt pct Co SMA, (d) Cu-Al-Ni-1 wt pct Co SMA.

due to the reduction in the formation and propagation of cracks as indicated in Figures 11(b) through (d). However, the variations in the fracture modes are attributed to the amount of elastic anisotropy at the grain boundaries and the presence of the γ_2 phase in the microstructures of the modified alloys. Therefore, despite the small elastic anisotropy at the grain boundaries, dimple rupture still occurs, which represents the ductile fracture. We can conclude that the alloying element is one of the most important factors that can influence the amount of elastic anisotropy, and thus, the variation in amount of added alloy is able to alter the fracture feature of the alloys. On the other hand, the fracture surface of the alloys can also be affected by the structural compounds, for instance, parent phases, precipitates, and intermetallic compounds along with their size and distribution into the matrix.^[49,50]

The microhardness values of the Cu-Al-Ni SMA with different Co contents are shown in Table V. The microhardness value substantially increased with the increasing Co content. The hardness value of the Cu-Al-Ni SMA was 223.6 MPa. However, the addition of 0.4 wt pct Co increased the hardness value considerably to 273 MPa. This phenomenon can be attributed to the maximum solubility of Co in the base alloy at ambient temperature in the equilibrium state. At this value, Co starts to precipitate within the Al-matrix and the grain boundaries, which was the main reason for the increase in hardness value. The FESEM micrographs of the Cu-Al-Ni- x Co ($x = 0.4, 0.7, \text{ and } 1$ wt pct) SMAs further confirmed the formation of the γ_2 phase on the matrix and grain boundaries as seen in Figures 2(b) through (d). Further

addition of Co (up to 0.7 wt pct) into the Cu-Al-Ni ternary alloy led to an increase in the hardness value to 329 MPa, due to the formation of more precipitates in the γ_2 phase. These precipitates act as obstacles to dislocation sliding, thus restricting further grain growth. When the content of Co reached 1 wt pct, the hardness value increased to 345 MPa due to the additional refining effect of Co on the alloys associated with the high volume fraction of γ_2 phase in the microstructure.

2. Shape memory effect

Under stress-free conditions, the low-symmetry martensite lattice can exist in several lattice correspondence variants, which are reflections or rotations of each other. Consequently, martensite can exist in many forms of microstructures depending on the thermomechanical history. The thermal-martensite is internally twinned, where twin-related variants create a coherent mirror image of the lattice across each twin boundary (special crystallographic planes). Some of the requirements for shape memory behavior are as follows^[51]: (1) the transformation between austenite and martensite occurs with little volume change and (2) the distortional strains relative to austenite are relatively small, typically on the order of 10 pct. In other words, the structural change can occur due to small coordinated shifts of the atomic positions without diffusion or plasticity. The shape memory effect arises from the fact that martensite can arrange itself into a self-accommodating, finely twinned (heterogeneous) structure with little or no macroscopic strain relative to austenite. Hence, upon cooling from austenite to martensite, little, if any, strain (or shape

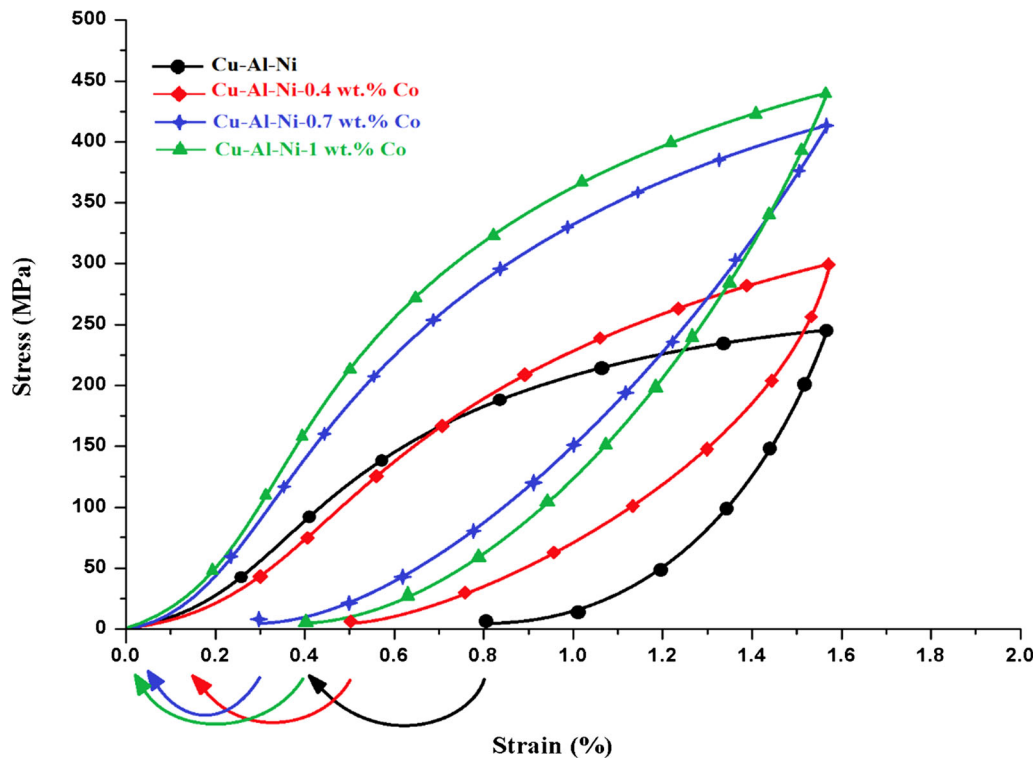


Fig. 12—Shape memory effect curves of the alloys performed at 373 K (100 °C), followed by preheating to 573 K (300 °C) to obtain shape recovery.

change) is usually observed (unless the material has been heavily processed to have the so-called two-way shape memory effect). We call this a self-accommodated form of thermal-martensite.^[52]

Figure 12 shows the strain recovery by the shape memory effect of Cu-Al-Ni SMAs as a result of varying the amount of Co, values of which are given in Table V. Clearly, the strain recovery of the base alloy has increased dramatically when the amount of Co addition increases, and the modified alloys have exhibited strain recovery by SME: about 95 pct of the original shape. Throughout, it was observed that ϵ^{SME} is mainly affected by the addition of alloy elements, because these elements are able to control the amount of austenite \rightleftharpoons martensite transformation. Therefore, any residual martensite in the austenite phase will influence the strain recovery by SME. Furthermore, imperfections such as dislocation and quenched-in vacancies may also affect strain recovery by SME, which caused pinning of the martensite plate-like/needle-like movements, thus restraining the transformation and reduction of strain recovery. However, it has been observed at higher percentages of Co addition that strain recovery has exhibited almost complete shape recovery. This may be attributed to the ease of occurrence of austenite \rightleftharpoons martensite transformation, as well as the formation of the γ_2 phase with a higher proportion of area fraction in the Cu-Al-Ni-1 wt pct Co SMA.

III. CONCLUSIONS

1. Microscopic observation shows that the addition of Co to Cu-Al-Ni SMA contributes to producing what is known as the γ_2 phase, which represents the $Al_{75}Co_{22}Ni_3$ phase. In addition, the morphology, the structure, and the order of the martensite phase varied after Co addition. Moreover, it was discovered that after increasing Co addition to 1 wt pct, the volume fraction of the γ_2 phase increased.
2. The addition of Co to Cu-Al-Ni SMA influences these phase transformation temperatures in particular. Furthermore, it was found that the highest transformation temperatures came with a 1 wt pct of Co as a result of the high proportion of the γ_2 phase in the microstructure. Nevertheless, thermodynamic parameters such as enthalpy and entropy varied after Co addition.
3. When the Co is added to Cu-Al-Ni SMA, the fracture stress-strain curve increases and reaches its maximum values with 1 wt pct Co. This may be attributed to the presence of a high-volume fraction of the γ_2 phase that reduces the mobility of dislocation, thus increasing the strength and ductility of the alloy. With the addition of Co, the hardness values increase due to the existence of the γ_2 phase.
4. Shape recovery improves after Co addition, while strain recovery increases from 50 to 95 pct. These improvements are due to the presence of the γ_2 phase together with the variations in the structures and morphologies of Cu-Al-Ni SMA after Co addition.

ACKNOWLEDGMENTS

The author(s) would like to thank the Malaysian Ministry of Higher Education (MOHE) and Universiti Teknologi Malaysia for providing the financial support and facilities for the current research, under Grant No. R.J130000.7824.4F150.

REFERENCES

1. V. Gandhi and B.S. Thompson: *Smart Materials and Structures*, Springer, London, 1992.
2. K. Otsuka and C.M. Wayman: *Shape Memory Materials, Reprint*, Illustrated ed., Cambridge University Press, Cambridge, 1999.
3. Z. Nishiyama, M.E. Fine, and C.M. Wayman: *Martensitic Transformation*, Academic Press, New York, 1978.
4. A. Ibarra, J.S. Juan, E.H. Bocanegra, and M.L. Nó: *Mater. Sci. Eng. A*, 2006, vols. 438–440, pp. 782–86.
5. V. Recarte, J.I. Pérez-Landazábal, M.L. Nó, and J. SanJuan: *Mater. Sci. Eng. A*, 2004, vol. 370, pp. 488–91.
6. J. Font, E. Cesari, J. Muntasell, and J. Pons: *Mater. Sci. Eng. A*, 2003, vol. 354, pp. 207–11.
7. J.I. Pérez-Landazábal, V. Recarte, V. Sánchez-Alarcos, M.L. Nó, and J.S. Juan: *Mater. Sci. Eng. A*, 2006, vols. 438–440, pp. 734–37.
8. V. Sampath: *Smart Mater. Struct.*, 2005, vol. 14, pp. S253–60.
9. J.S. Lee and C.M. Wayman: *Trans. Jpn. Inst. Met.*, 1986, vol. 27, pp. 584–91.
10. M.A. Morris and S. Gunter: *Scripta Metall. Mater.*, 1992, vol. 26 (11), pp. 1663–68.
11. U. Sari and T. Kırdır: *Mater. Charact.*, 2008, vol. 59, pp. 920–29.
12. K. Yildiz and M. Kok: *J. Therm. Anal. Calorim.*, 2014, vol. 115, pp. 1509–14.
13. Z. Karagoz and C.A. Canbay: *J. Therm. Anal. Calorim.*, 2013, vol. 114, pp. 1069–74.
14. Y. Sutou, T. Omori, K. Yamauchi, N. Ono, R. Kainuma, and K. Ishida: *Acta Mater.*, 2005, vol. 53, pp. 4121–33.
15. Y. Itsumi, Y. Miyamoto, T. Takashima, K. Kamei, and K. Sugimoto: *Adv. Mater. Res.*, 1991, vols. 56–58, pp. 469–74.
16. M.A. Morris: *Scripta Metall.*, 1991, vol. 25, pp. 1409–14.
17. K. Adachi, K. Shoji, and Y. Hamada: *ISIJ Int.*, 1989, vol. 29, pp. 378–87.
18. D.W. Roh, J.W. Kim, T.J. Cho, and Y.G. Kim: *Mater. Sci. Eng. A*, 1991, vol. 136, pp. 17–23.
19. M.A. Morris and T. Lipe: *Acta Metall. Mater.*, 1994, vol. 42, pp. 1583–94.
20. S. Saud, E. Hamzah, T. Abubakar, and S. Farahany: *J. Mater. Eng. Perform.*, 2013, vol. 23, pp. 255–61.
21. S.N. Saud, E. Hamzah, T.A. Abu Bakar, and A. Abdolahi: *Mater. Sci. Technol.*, 2014, vol. 30, pp. 458–64.
22. S. Saud, E. Hamzah, T. Abubakar, M. Zamri, and M. Tanemura: *J. Therm. Anal. Calorim.*, 2014, vol. 118, pp. 111–12.
23. U. Sari and İ. Aksoy: *J. Alloy. Compd.*, 2006, vol. 417, pp. 138–42.
24. U. Sari: *Int. J. Miner. Metall. Mater.*, 2010, vol. 17, pp. 192–98.
25. S.H. Chang: *Mater. Chem. Phys.*, 2011, vol. 125, pp. 358–63.
26. N. Bergeon, G. Guenin, and C. Esnouf: *J. Phys. IV Fr.*, 1997, vol. 7, pp. C5-125–30.
27. M. Eskil and N. Kayali: *Mater. Lett.*, 2006, vol. 60, pp. 630–34.
28. Y. Aydogdu, A. Aydogdu, and O. Adiguzel: *J. Mater. Process. Technol.*, 2002, vol. 123, pp. 498–500.
29. C.M. Friend: *Scripta Metall.*, 1989, vol. 23, pp. 1817–20.
30. Q. Xuan, J. Bohong, and T.Y. Hsu: *Mater. Sci. Eng.*, 1997, vol. 93, pp. 205–11.
31. R.J. Salzbrenner and M. Cohen: *Acta Metall.*, 1979, vol. 27, pp. 739–48.
32. O. Adiguzel: *Mater. Res. Bull.*, 1995, vol. 30, pp. 755–60.
33. Ş.N. Balo and N. Sel: *Thermochim. Acta*, 2012, vol. 536, pp. 1–5.
34. Y. Gwon-Seung, L.E.E. Jong-Kook, and J. Woo-Yang: *Trans. Nonferrous Met. Soc. China*, 2009, vol. 19, pp. 979–83.
35. B.D. Cullity and S.R. Stock: *Elements of X-ray Diffraction*, Prentice Hall, Upper Saddle River, 2001.
36. A.L. Patterson: *Phys. Rev.*, 1939, vol. 56, pp. 978–82.
37. S.Q. Zhang Xiangyang and Yu. Shouwen: *J. Mech. Phys. Solids*, 2000, vol. 48, pp. 2163–82.

38. X. Zhang, L. Brinson, and Q.-P. Sun: *Smart Mater. Struct.*, 2000, vol. 9, p. 571.
39. W. Wang, Z. Liu, J. Zhang, J. Chen, G. Wu, W. Zhan, T. Chin, G. Wen, and X. Zhang: *Phys. Rev. B*, 2002, vol. 66, p. 052411.
40. S. Saud, E. Hamzah, T. Abubakar, and H.R. Bakhsheshi-Rad: *J. Therm. Anal. Calorim.*, 2015, vol. 119, pp. 1273–84.
41. C. Tatar: *Thermochim. Acta*, 2005, vol. 437, pp. 121–25.
42. J. Ortín and A. Planes: *Acta Metall.*, 1989, vol. 37, pp. 1433–41.
43. S. Miyazaki, K. Otsuka, H. Sakamoto, and K. Shimizu: *Trans. Jpn. Inst. Met.*, 1981, vol. 22, pp. 244–52.
44. G. Motoyasu, M. Kaneko, H. Soda, and A. McLean: *Metall. Mater. Trans. A*, 2001, vol. 32A, pp. 585–93.
45. N. Yang, C. Laird, and D.P. Pope: *Metall. Trans. A*, 1977, vol. 8A, pp. 955–62.
46. H. Funakubo: *Shape Memory Alloys*, CRC Press LLC, Boca Raton, 1987.
47. K. Otsuka, H. Sakamoto, and K. Shimizu: *Acta Metall.*, 1979, vol. 27, pp. 585–601.
48. S. Husain and P. Clapp: *J. Mater. Sci.*, 1987, vol. 22, pp. 2351–56.
49. Q.P. Yang, L. Sun, and Y.Z. Feng: *Appl. Mech. Mater.*, 2011, vols. 71–78, pp. 1707–10.
50. S. Gollerthan, M. Young, A. Baruj, J. Frenzel, W. Schmahl, and G. Eggeler: *Acta Mater.*, 2009, vol. 57, pp. 1015–25.
51. K. Bhattacharya: *Microstructure of Martensite: Why it Forms and How it Gives Rise to the Shape-Memory Effect*, OUP, Oxford, 2003.
52. C.B. Churchill, J.A. Shaw, and M.A. Iadicola: *Exp. Tech.*, 2009, vol. 33, pp. 70–78.